Electronic Supplementary Material (ESI) for Journal of Materials Chemistry A.

Supplementary information

A breath of fresh air for atmospheric CO_2 utilisation: plasmon-assisted preparation of cyclic carbonate at ambient conditions

Olga Guselnikova[1,2], Pavel Postnikov[1,2,*], Jiri Kosina[3], Zdenla Kolska[4], Andrii Trelin[1], Vaclav Svorcik[1], Oleksiy Lyutakov[1,2*]

[1] *Department of Solid State Engineering, University of Chemistry and Technology, 16628 Prague, Czech Republic*

[2] *Research School of Chemistry and Applied Biomedical Sciences, Tomsk Polytechnic University, 634049 Tomsk, Russian Federation*

[3] *Central laboratories, University of Chemistry and Technology, 16628 Prague, Czech Republic*

Content

Experimental part

Materials

All chemicals used were of analytical grade or of the highest purity available to us. $HAuCl_4$ (99.995 %), trisodium citrate dihydrate (Na_3CA, > 98 %), methanol (reagent grade, ≥ 99 %), diethyl ether, deionised water, p-Toluenesulfonic acid monohydrate (ACS reagent, ≥98.5 %), 4-Aminophenethyl alcohol (98 %), 2-Bromopropionyl bromide (97 %), 1,5,7-Triazabicyclo[4.4.0]dec-5-ene (98 %), Triethylamine (> 99 %), (±)-Propylene oxide (puriss. p.a., ≥ 99.5 %), 1,2-Epoxybutane (99%) were purchased from Sigma-Aldrich and used without further purification. All glassware was thoroughly cleaned with freshly prepared 3:1 HCl/HNO_3 (aqua regia) and rinsed thoroughly by water prior use.

Preparation of AuNPs

Gold nanospheres (AuNPs) were prepared by the modified Turkevich method. In 250 mL round bottomed flask, 1 mL of $HAuCl_4$ (100 mg in 10 mL) and 2.5 mL of Na_3CA (284.9 mg in 25 mL) were added to 100 mL of boiling water. Heating was continued for 10 min during which time the solution become red. After cooling to room temperature (RT), the AuNPs solution was used as prepared.

Diazotation and in-situ modification (I)

Modification of AuNPs using in situ generated diazonium was carried out in a mixture of water and methanol (1/1) at room temperature. *Tert*-butyl nitrite was slowly added (20 μL, 0.1 mmol) to the solution of p-TsOH (0.019 g, 0.1 mmol) in methanol (2 mL), Next, the 4-Aminophenethyl alcohol 0.05 mmol (0.007 g) was added in 4 steps to the reaction mixture over 1 min. The mixture was left to react for about 1.5 hours prior to the functionalisation. Then 2 ml of water was added to the reaction mixture was left for 10 min. After 40 ml of freshly prepared AuNPs were added and stirred for 1 hour. Finally, AuNPs were purified by centrifugation and washing with ethanol and (7500 rpm, 15 min) three times. Resulting AuNPs were suspended in 5 ml of tert-butyl toluene. The −OH terminated gold surfaces are abbreviated as AuNPs-CH_2-OH.

Acylation with 2-bromopropionyl bromide(II)

AuNPs-CH_2-OH with the terminal hydroxyl groups were treated with 2-bromopropionyl bromide (0.1 M, dichloromethane) in the presence of TEA (0.12 M) for 40 min to produce bromo-terminated ester groups. Then AuNPs were purified by centrifugation and washing with dichloromethane and (7500 rpm, 15 min) three times. Resulting AuNPs were suspended in 5 ml of tert-butyl acetonitrile. The −Br terminated gold surfaces are abbreviated as AuNPs−Br.

Immobilisation of 1,5,7-Triazabicyclo[4.4.0]dec-5-ene (III)

AuNPs−Br were further treated with 1 mM solution of 1,5,7-Triazabicyclo[4.4.0]dec-5-ene (TBD) in acetonitrile for 2 hours. Then, AuNPs were purified by centrifugation and washing with acetonitrile and methanol and (7500 rpm, 15 min) three times. Resulting AuNPs were suspended in 3 ml of propylene oxide or 1,2-epoxybutane. The −TBD terminated gold surfaces are abbreviated as AuNPs-TBD.

Capturing of CO_2 from CO_2/N_2 mixtures

AuNPs-TBD (3 mg) was dispersed in 3 ml of methanol at RT under stirring and evacuated. CO_2 or CO_2/N_2 mixture was introduced into the reaction mixture from a regular balloon (approximately 3 L) via the needle. The suspension was bubbled for 30 minutes. After, AuNPs-TBD were separated by centrifugation, deposited on SiO_2 wafer (0.5*0.5 cm^2) and SERS spectra were immediately measured 3 time on different positions.

Catalyst leaching experiments

TBAB (50 mg, 0.15 mmol) was added to the suspension of Au-TBD (3 mg) in 3 ml of epoxide at RT and mixture was treated in the ultrasound bath for 1 minute. CO_2 was introduced into the reaction mixture from a regular balloon (approximately 3 L of CO_2) via the needle with the preliminary filling of reaction flask by CO_2. The reaction mixture was illuminated with LED (780 nm, 40 mW/cm^2) under stirring for 12 hours. Then, Au-TBD were removed from the reaction mixture by centrifugation (7000 rpm, 30 min) and the reaction mixture was illuminated with LED (780 nm, 40 mW/cm^2) further 12 hours. The probes of the reaction mixture were taken after different times and analysed by GC.

Measurement techniques

UV-Vis spectra were measured using Spectrometer Lambda 25 (Perkin-Elmer) in 300-1000 nm wavelength range. Raman spectra were measured on portable ProRaman-L spectrometer with 785 nm excitation wavelengths (laser power 40 mW, Integrations 100, average 1). TEM images of nanoparticles were obtained on JEOL JEM-1010 Instrument operated at 80 kV (JEOL Ltd., Japan). Agilent 7010 GC was equipped with a flame ionization detector (FID) and a Rxi-5ms column (20 m x 0.18 mm x 0.30 um). GC program: 40°C (3 min) - > 15°C/min - > 290°C (5 min), carrier gas: Helium, constant flow 0.7 ml/min, spray: 1 µl, split 1:10, temperature 250°C. ^{1}H NMR spectra were recorded on Bruker Avance III™ (500 MHz) spectrometer. Chemical shifts are given in parts per million (δ/ppm), referenced to dimethylsulfoxide (2.51) as an internal standards. All coupling constants are absolute values and are expressed in Hertz (Hz). The description of signals includes: s = singlet, d = doublet, t = triplet. ^{13}C NMR spectra were recorded on Bruker Avance III™ (500 M Hz) spectrometers. Elemental organic analysis was performed on Vario EL Cube (Elementar

GmbH). Intensity of LED irradiation was measured by Integrating Sphere Photodiode Power Sensors (Throrlabs, S142C).

For dynamic light scattering and zeta potential measurements Au-TBD in H_2O/MeOH (1/1) were placed in the cuvette for DLS and zeta-potential measurements using a Malvern Zetasizer Ultra. A total of 15 scans, each with duration of 20 s, were accumulated for each sample. Zeta potential data were obtained using a monomodal acquisition and fit according to the Smoluchowski theory. All the samples were analysed in triplicate.

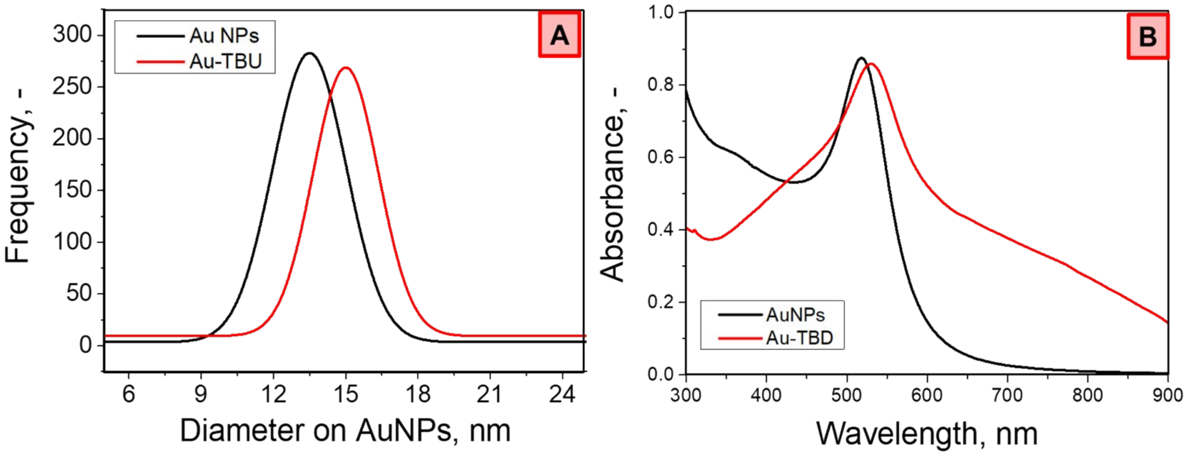

Figure S1 (A) - particles size distribution calculated from TEM images; (B) - UV-Vis spectra of Au, Au-TBD in water.

Confirmation of Au-TBD grafting of AuNPs

SERS spectra of bare AuNPs do not demonstrate any significant peak (Fig. 2C), while modification with 4-(2-hydroxyethyl)benzene diazonium tosylate, lead to the appearance of new Raman signals described in Tab S1, confirming the successful realisation of step I. Prepared AuNPs are abbreviated as AuNPs-CH_2-OH as mentioned above. XPS spectra of AuNPs-CH_2-OH after diazonium modification demonstrated an increase of C1s (285.4 eV) and O1s (530.6 eV) peaks simultaneously with a decrease of Au4f (85.2-88.8 eV) peak due to the attachment of organic moieties. The completion of step (ii), i.e. acylation of terminated groups by 2-bromopropionyl bromide, was confirmed by SERS measurement and the appearance of new peaks assigned to asymmetric -CH_3 deformational vibrations and C-Br stretch. The final step leading to the covalent immobilisation of nitrogen-containing organic base TBD was monitored by SERS and XPS. On the SERS spectra, we clearly see multiple peaks assigned to C-N stretching vibration. XPS spectra show the presence of 14 % of N in combination with C, the concentration of which increased to 5 at. %. Moreover, deconvolution of N1s peaks demonstrate peaks at 403 and 403.8 eV corresponding to the secondary and tertiary amines (Fig. S2).

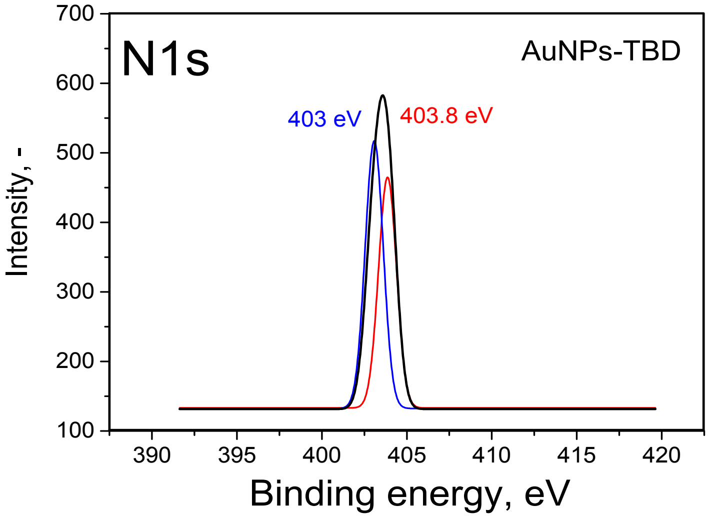

Figure S2 Deconvolution of N1s XPS region, measured from Au-TBD.

Table S1. Assignation of Raman bands after subsequent steps of TBD grafting to AuNPs surface

Peak position, cm^{-1}	Assignation
AuNPs-CH_2-OH	
1585	C=C str vib
1563	C=C str vib
1435	In plane OH bending, CH_2 def vib
1317	CH_2 wagg, CH def vib
1217	CCO str, =CH in plane vib
1158	C-C skel vib, =CH in plane vib
1043	C-C skel vib, =CH in plane vib
982	CH_2 twist vib, =CH in plane vib
911	CH_2 twist vib, =CH out of plane vib
773	=CH out of plane vib,
682	O-H out of plane def vib, C-O def vib, Ar ring def
585	O-H out of plane def vib, C-O def vib, Ar ring def
474	C-C skel vib
AuNPs-Br	
1585	C=C str vib
1484	OCH_2 def vib, asym CH_3 def vib
1453	OCH_2 def vib, asym CH_3 def vib

1365	asym CH_3 def vib
1326	asym CH_3 def vib
1245	CH_2 wagg, CH def vib, asym CH_3 def vib
1117	CH_3 rocking vib, C-C skel vib, =CH in plane vib
1045	CH_3 rocking vib, C-C skel vib, =CH in plane vib
965	=CH in plane vib
692	C-Br str
645	C-Br str
522	C-Br vib
474	C-C skel vib
AuNPs-TBD	
1636	C-N str (C=N)
1564	N-H vib
1462	OCH_2 def vib, asym CH_3 def vib
1414	OCH_2 def vib, asym CH_3 def vib
1311	C-N str vib
1155	CNC str
1082	C-N vib
1053	N-H wag vib
816	str CCN sym
682	CH out of plane
486	C-N-C bend
279	CH_3 vib

.

Calculation of TBD loading on AuNPs

After preparation, the resulting AuNPs were suspended in acetone (the mass of Au-TBD was established to be 3±0.1 µg mg per 5 ml of solvent, using gravimetric analysis with Excellence XPR Ultra-Microbalance XPR2U). To estimate the amount of attached TBD organic elemental analysis was performed on the as-prepared nanoparticles and those after multi step modification. The change in nitrogen content after the modification was used to calculate the TBD loading in mmol per g of AuNPs.

Table S2 Data of organic elemental analysis obtained from Au and Au-TBD.

Sample	**Element concentration (at %)**	
	N	***C***
AuNPs	0	0.3
Au-TBD	0.3	3.4

The elemental composition of the grafted TBD groups allowed us to establish 0.07 mM of functional groups per 1 g of AuNPs. For the calculation of number of TBD molecules per 1 AuNPs, we considered the average radius 6.3 nm leading to volume 2143.5 nm^3 or 41.5×10^{-18} g (using density of AuNPs 19.32 g/cm^3). This means that single AuNP contains approximately 3×10^{-21} mM of TBD or 1800 TDB molecules.

Characterisation of Au-TBD-CO$_2$ adduct

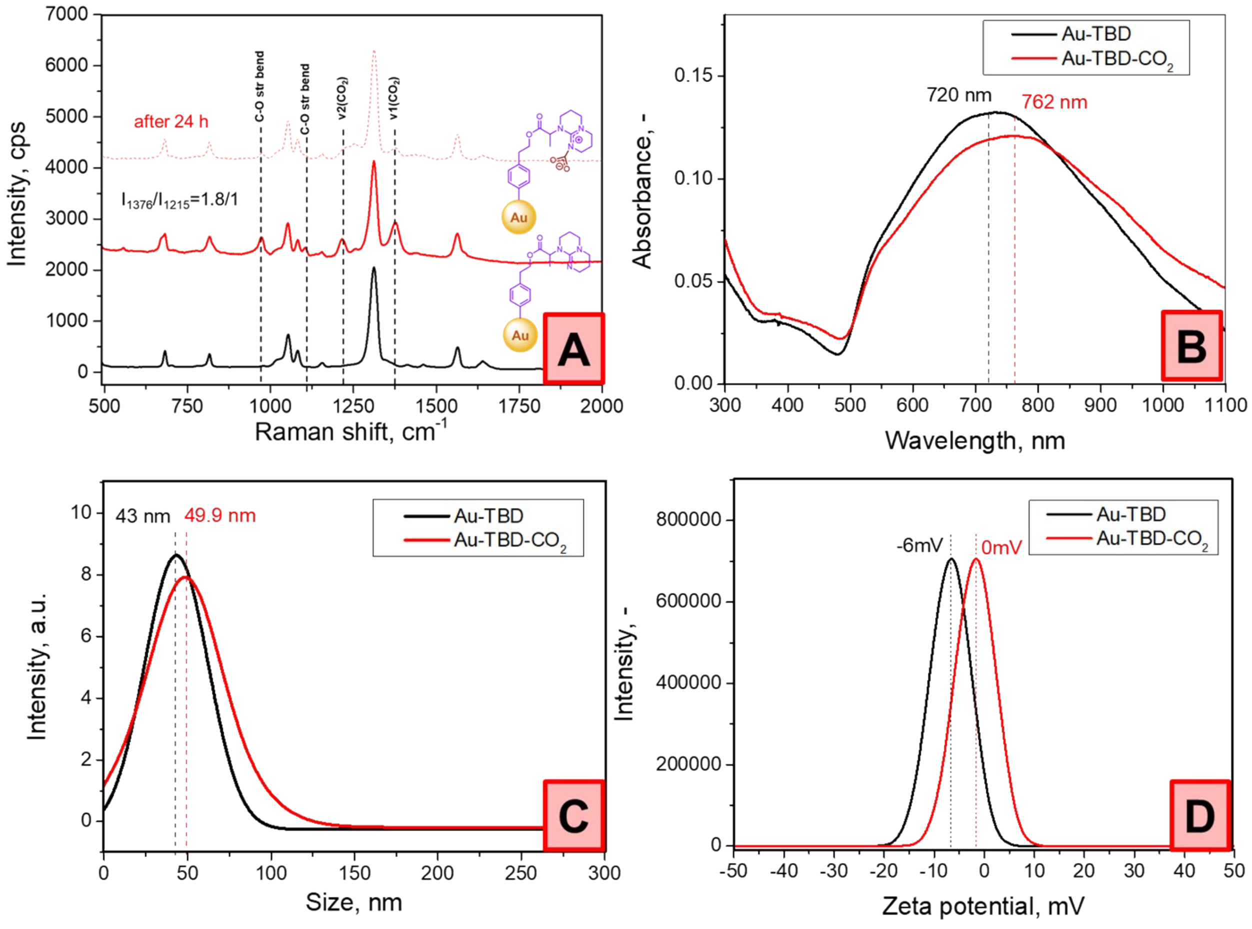

Figure S3 Characterisation of Au-TBD-CO$_2$ zwitterionic complex before and after CO$_2$ entrapping (3 minutes bubbling): (A) - SERS spectra; (B) - UV-Vis absorption spectra, measured in BO; (C) -

DLS-measured nanoparticles size distribution; (D) - measured by zeta potential nanoparticles surface charge

Related discussion

To check the availability of immobilised TBD for CO_2 entrapping, we suspended the Au-TBD in the CO_2 saturated acetone for 30 min and further isolated them to immediate SERS measurements. The recorded SERS spectra (Fig. S3A) indicate the appearance of typical for CO_2 vibration bands - ν_1 (1377 cm^{-1}) and ν_2 (1214 cm^{-1}), previously observed on similar adducts. However, we additionally observed the suppression of C-N str (C=N) peak (1636 cm^{-1}) and the appearance of new $^{+}$C-N stretching vibration (1106 cm^{-1}) related to imine charged derivative. Simultaneously 972 cm^{-1} peak appears which can be assigned to the negatively charged C-O stretch band.

In addition, the effect of AuNPs-TBD-CO_2 adduct formation was investigated using UV-Vis absorption spectroscopy, DLS and z-potential measurements. The UV-vis absorption spectrum of pristine Au-TBD adduct (Fig. S3B) is slightly red-shifted after CO_2 entrapping, indicating the changes of metal nanoparticles dielectric environment. The DLS-measured nanoparticles distribution (Fig. S3C) indicates the significant increase of "apparent" nanoparticles size, probably due to the increase of effective hydrodynamic radius after CO_2 entrapping. Finally, zeta-potential measurements (Fig. S3C) of pristine Au-TBD indicate the presence of a slightly negative charge on Au-TBD (probably, due to the grafting of organic base - nitrogen-containing heterocyclic compound). After the formation of zwitterionic complex, the surface charge is slightly shifted, indicating the charge redistribution near the nanoparticles surface. So, summarising the results of SERS, UV-Vis, DLS and z-potential measurements we can claim that spontaneous CO_2 capture with the formation of zwitterionic adduct occurs. However, the formed adduct is stable and cannot react with organic epoxides without external triggering. Commonly, the heating of reaction mixture and increase of pure CO_2 pressure is required at this stage for the activation of similar complexes (Table S2). We further focus our attention on the alternative way – utilisation of plasmon-assistance, which allow us to perform reaction at RT without CO_2 pressure increasing.

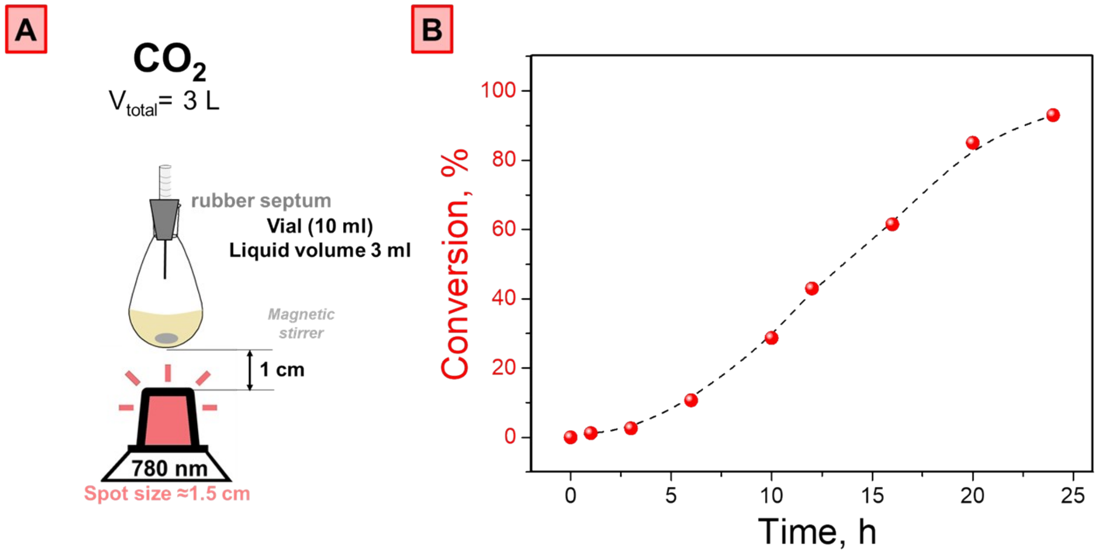

Figure S4 (A) - schematic representation of experimental setup for CO_2 plasmon-assisted cycloaddition (*entries 1-5 and 7-11*); (B) - dependence of 1,2-epoxybutane conversion on the reaction time (using 3 mg of Au-TBD, red dots) with the simultaneous monitoring of reaction temperature (blue dots).

Related discussion

For the plasmon-induced cycloaddition reaction, the 10 ml vial (sodium silicate glass outer diameter 2 cm, 4 cm height, 1 mm thick) was filled by the epoxide (3 ml) and Au-TBD. The LED source (780 nm, 40 mW/cm^2, product number M780LP1, Thorlab) was set up vertically at 1 cm distance from vial bottom (Fig. S4). The spot size of LED was 1.5 cm (emitter size 3 mm) at this distance, and the light irradiance “first glass window” was measured to be 40 mW/cm^2 by Integrating Sphere Photodiode Power Sensors (Thorlabs, S142C). The chemically inert balloons (wall thickness 12 mm, maximum volume 7 L) filled with ≈ 1 L of CO_2 (SIAD, E290) was inserted into septum (slight positive pressure can be maintained in the balloon). Irradiation and stirring or reaction mixture were started simultaneously. The balloons were replaced 3 times by fresh CO_2 after visual balloon emptying, and the final volume of added CO_2 was ≈3L.

Spectroscopic characterisation

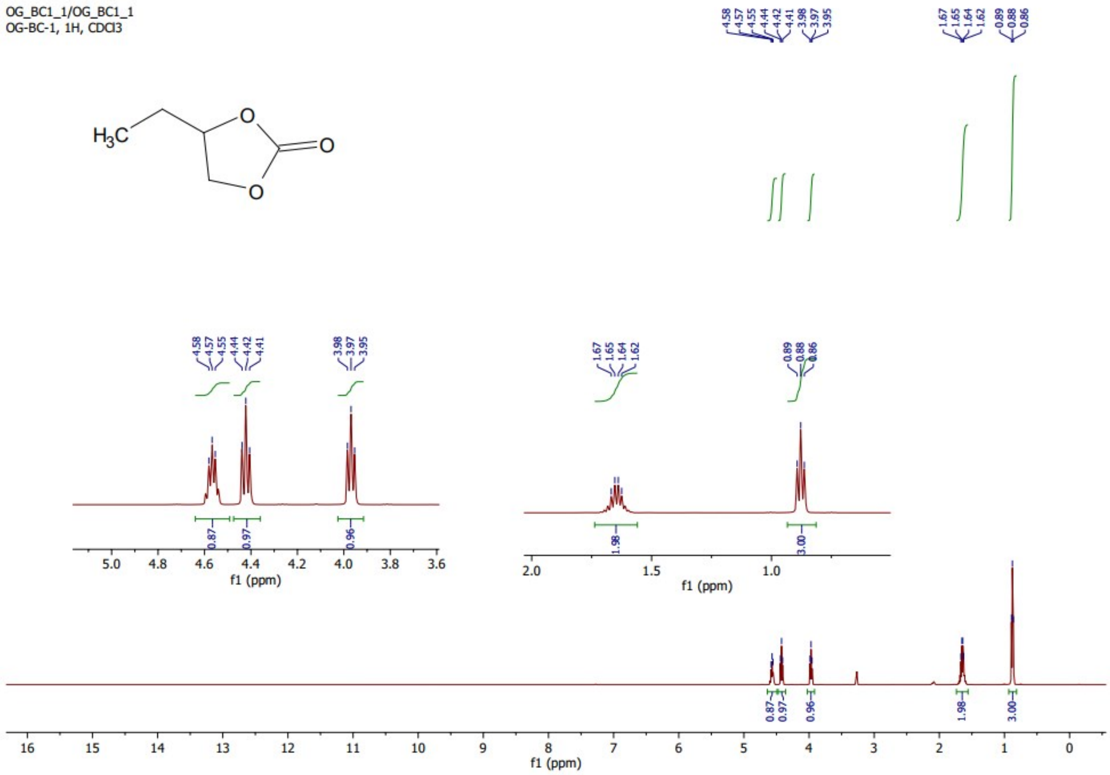

Figure S5 ^{1}H NMR spectra of butylene carbonate

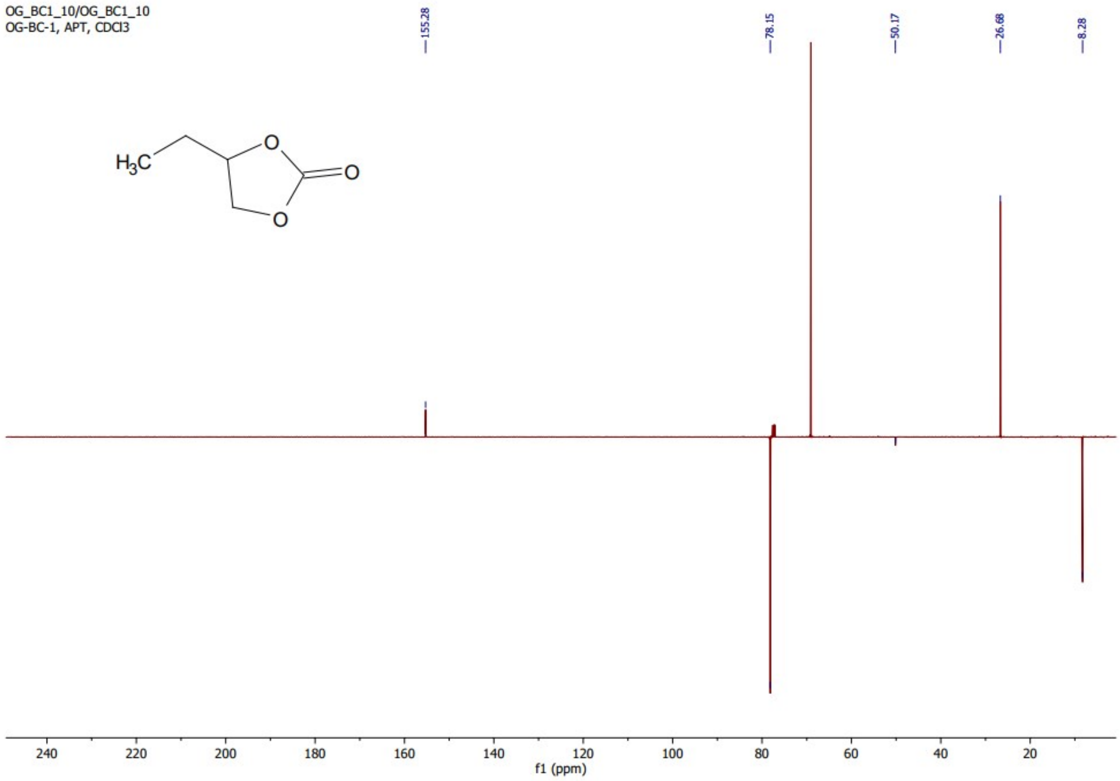

Figure S6 ^{13}C NMR spectra of butylene carbonate.

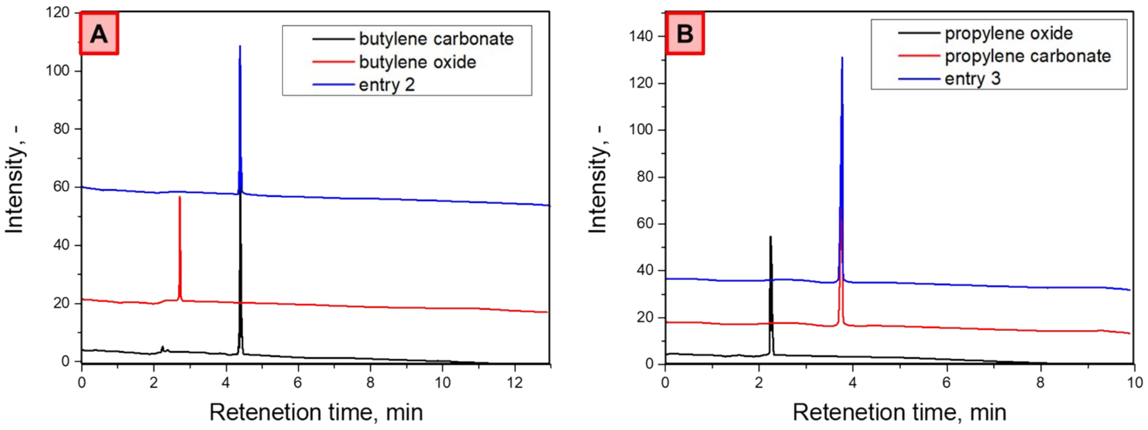

Figure S7 (A) - GC chromatogram obtained from entry 2 (formation of butylene carbonate); (B) - GC chromatogram obtained from entry 3 (formation of propylene oxide). Both chromatograms show the “marker” signals from corresponded epoxides and carbonates.

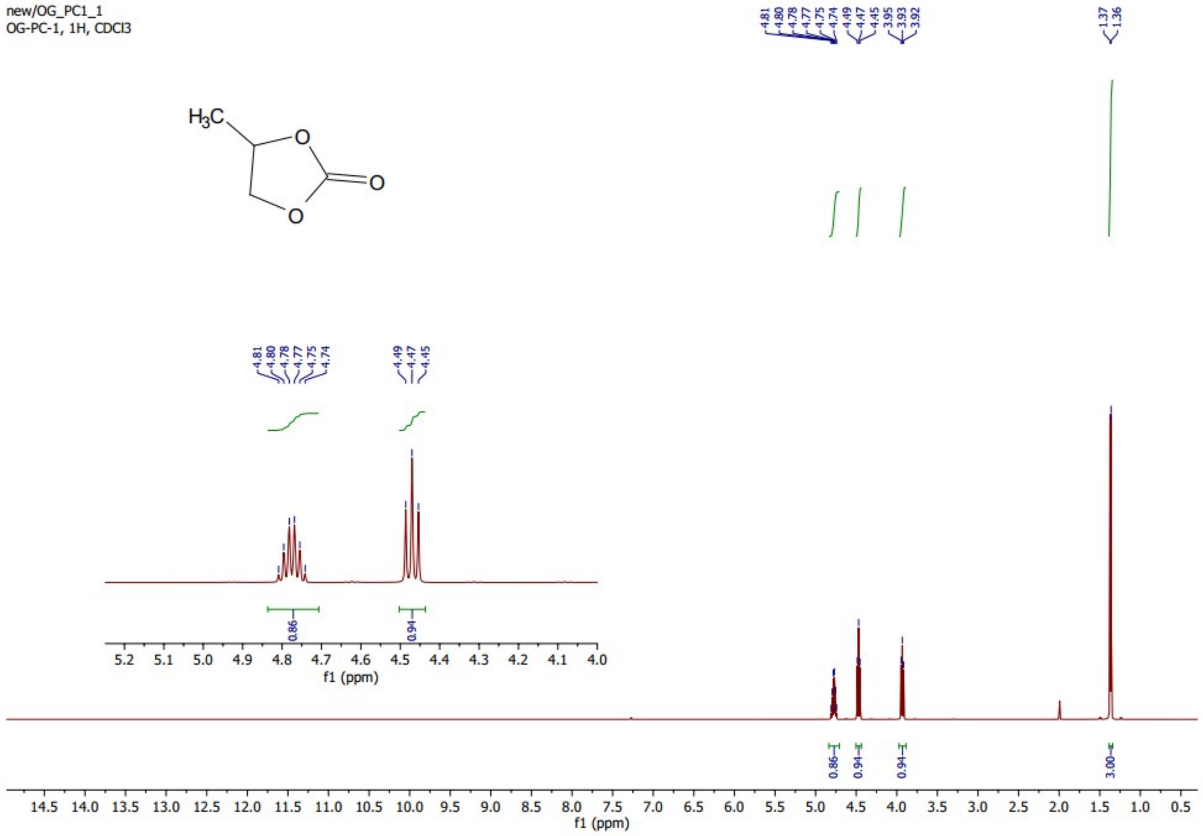

Figure S8 ^{1}H NMR spectra of propylene carbonate.

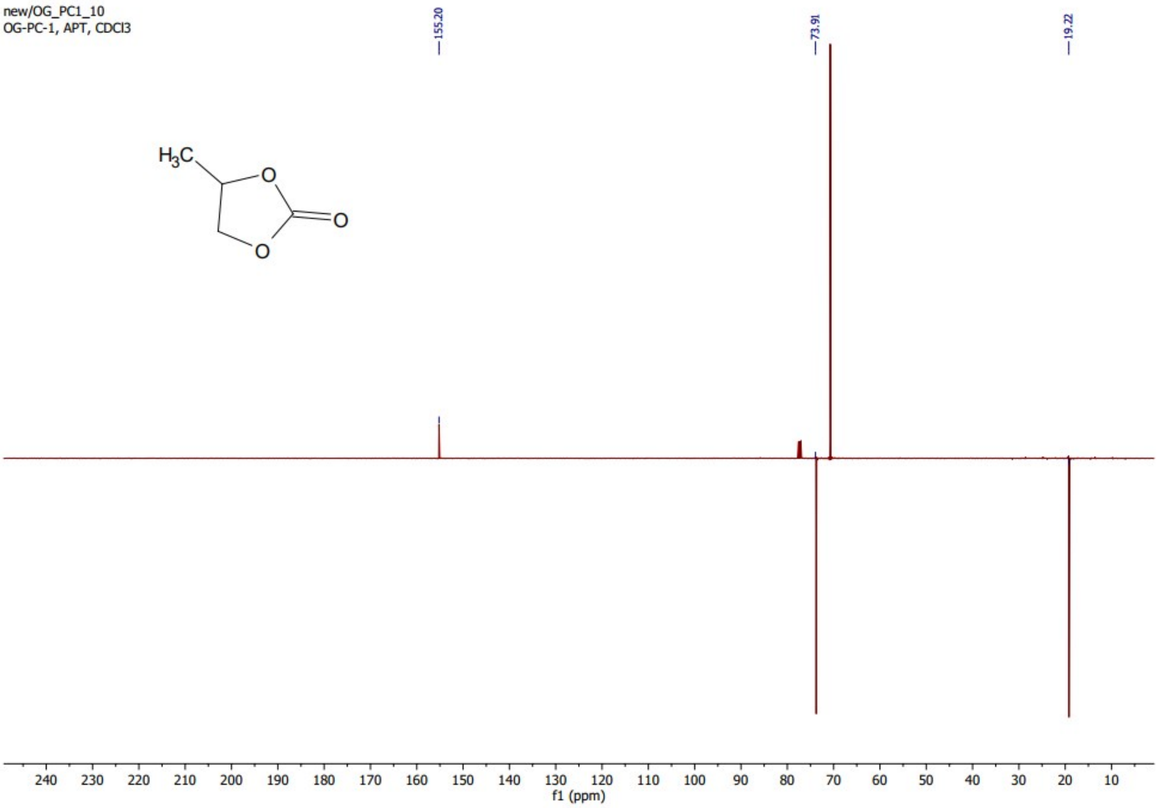

Figure S9 ^{13}C NMR spectra of propylene carbonate.

Table S2 Comparison of experimental conditions used for CO_2 cycloaddition using nitrogen-containing organic base: previous results vs our work.

Catalyst	**CO_2 source**	**Temperature, °C**	**Pressure, bar**	**Time of reaction, h**	**Yields, %**	**Reference**
DBU-cellulose	balloon	120	20	2	92	[S1]
TBD/SiO_2	balloon	23	20	20	99	[S2]
Methyl-TBD	balloon	140	50	20	98	[S3]
TBD based ionic liquid	balloon	120	100	3	99	[S4]
Covalent organic polymer	balloon	100	1	36	99	[S5]
MOF	balloon	23	1	48	96	[S6]
AuNPs-TBD	**balloon**	**23**	**1**	**24**	**97**	**This work**
AuNPs-TBD	**air**	**23**	**1**	**48**	**69**	**This work**

Estimation of plasmon-heating potential impact

To estimate the order of magnitude of local heat effect, absorption cross-sections of nanoparticle dimer were calculated with SCUFF-EM [S7] software that implements the boundary element method. In the second step, the temperature profile across nanoparticle dimer was computed from absorption cross-sections, taking into account the irradiance and macroscopic thermal parameters of the surrounding (1,2-epoxybutane [S8, S9]. The interfacial thermal conductance of nanoparticle-liquid interface was assumed to be 100 MW/K·m^2, according to the literature [S10]. Uniform heat distribution inside nanoparticle was also assumed, taking into account the large gold thermal conductivity (compared to the conductivity of surrounding) and “small” particle size. To evaluate whether assumption of uniform heat generation in NP are meaningful, the nanoparticles dimer was additionally simulated with BUFF-EM volume-integral-equation solver [S11], which allows calculation of density of heat generation inside the system of interest – i.e. potential impact of spontaneous hot spots formation in the case of plasmonic dimer or multimer appearance, which can led to enhanced heat generation.

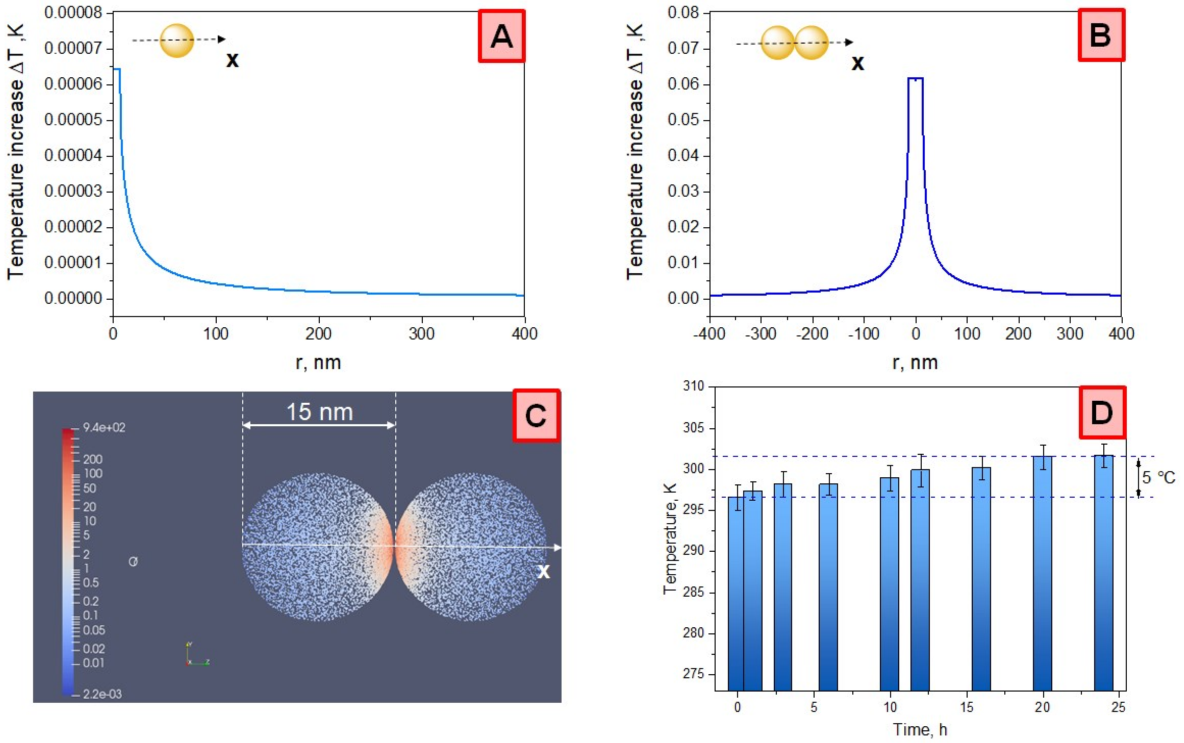

Figure S10 (A) - local temperature profile around single nanoparticle; (B) - local temperature profile assuming enhanced heat generation in nanoparticles dime case; (C) – normed heat generation density; (D) - monitoring of reaction temperature during CO_2 plasmon-induced cycloaddition. BAD A

Related discussion

Numerical simulation of temperature increase – nanoparticles dimer and hot spot cases. Local temperature profile obtained by solving the described system with finite element method is shown in the Fig. S10A. The expected temperature increase is on the order of 10^{-5}K, which is far from chemical significance. To evaluate the potential impact of plasmonic hot spots formation and related non-uniform heat generation (this situation is presented in Fig. SJJJC) meaningful, the nanoparticles dimer was additionally simulated with BUFF-EM volume-integral-equation solver [S11]. Obtained density of heat generation is presented in Fig. SJJJJC, why the results of calculation are shown in the Fig. S10B as a normalised heat generation value (temperature profile acrioss dotted line in Fig. S10C). Indeed, temperature increase in hor spot is greater, than in previous case (Fig. S10A vs Fig. S10B) - the local heat generation density was found to be almost in 10^3 times higher in the hotspot. However, even assuming this value, the absolute temperature increase is still less 0,1K (Fig, S10B). Thus, even under overoptimistic assumptions of optimal absorption and enhanced local heat generation, the thermal effects are still too small to justify the experimental data.

Experimental temperature estimation results of additional experimental tests of temperature tracking by miniaturised leaf thermocouple immersed in the reaction mixture suspension are presented in Fig. S10D. Obtained values revealed the increase of the suspension temperature by ≈5 °C within the error bar after 24 hours of irradiation in the stated above experimental conditions. So, even the "starting" temperature in Figs. S10 A, B does not overperform the 5 K.

To sum up, the results of numerical simulation and control experiments we can claim that plasmon local heating could not play the crucial role in the observed activity of Au-TBD catalyst and cycloaddition of CO_2 should be attributed to alternative plasmon-induced mechanisms, such as excited state energy transfer or innermolecular electron excitation [S12].

Impact of illumination stopping and catalyst catalyst leaching experiment

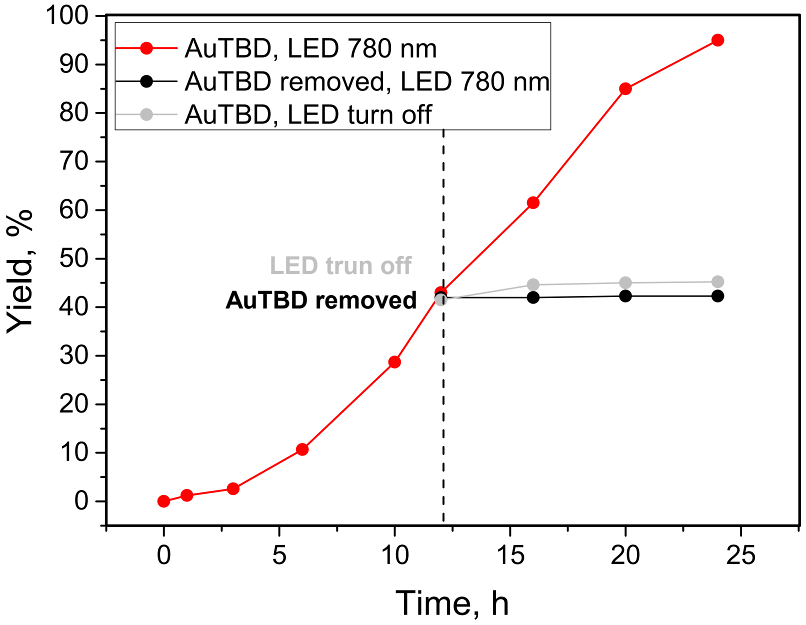

Figure S11 Results of catalyst leaching experiment – impact of LED turn-off and Au-TBD removing after reaction proceeding at 50%.

Related discussion

To monitor the possible catalyst leaching, the reaction of EB with CO_2 under plasmon triggering was stopped after 12 hours (43 % yield) and Au-TBD were removed by centrifugation (Fig. S11). The reaction was further continued with the filtrate under LED illumination. Alternative control experiments were performed by simple illumination interruption and keeping of reaction mixture in dark, without Au-TBD removing. In first case of we did observe significant increase in BC formation after Au-TBD removing (yield 43%). So, in absence of Au-TBD the reaction is completely suppressed and catalyst leaching does not occurs. In turn, illumination interruption also results in incomparable yield of 45%, additionally confirming the key role of plasmon triggering (Fig. S11).

Characterisation of Au-TBD after several cycles of utilisation

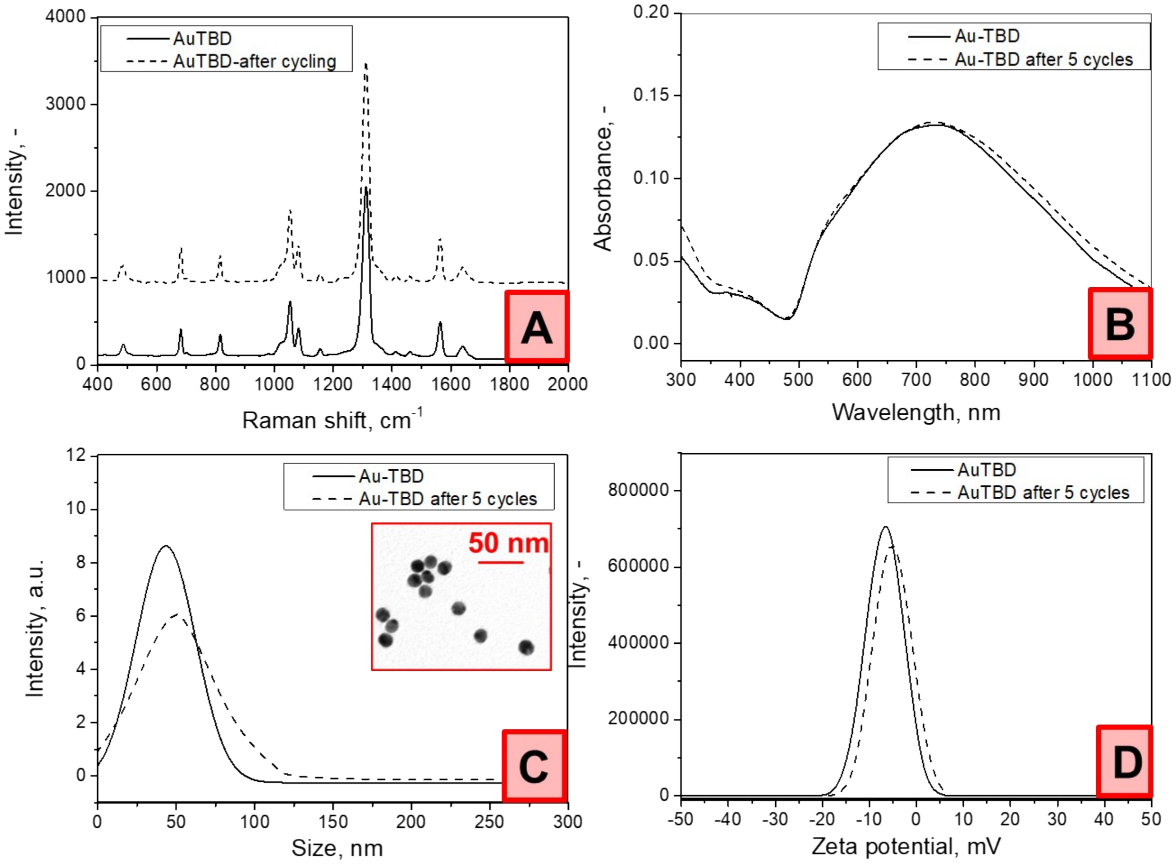

Figure S12 Characterisation of Au-TBD after several cycles of utilisation for CO_2 cycloaddition: (A) - SERS spectra, measured before and after 5 cycles of Au-TBD utilisation, (B) - UV-Vis absorption spectra of Au-TBD before and after 5 utilisation cycles; (C) - measured by DLS size distribution of Au-TBD after 5 cycles of utilisation (including the separation and redispersion steps); (D) - changes of surface charge on Au-TBD due to nanoparticles reutilisation.

Related discussion

The results of additional recyclability examination and Au-TBD potential degradation are presented in Fig. S12. According to SERS spectra (S12A) even after 5 cycles of reutilisation, no degradation or detachment of grafted cocatalysts was observed. After 5 cycles the SERS and UV-Vis spectra of Au-TBD demonstrate almost identical peaks with the conservation of position and intensities (Fig. S12B). In turn, DLS measurements show the widening of nanoparticles size distribution, which can be attributed to partial nanoparticles agglomeration and/or to the remaining absorbed CO_2 (Fig. S12C). In turn, we also observed a slight shift of surface charge values, after 5 cycles of nanoparticles reutilisation (Fig. S12D). Similarity of obtained surface charge distribution with previously observed (Fig. S3D) confirm the presence of absorbed CO_2.

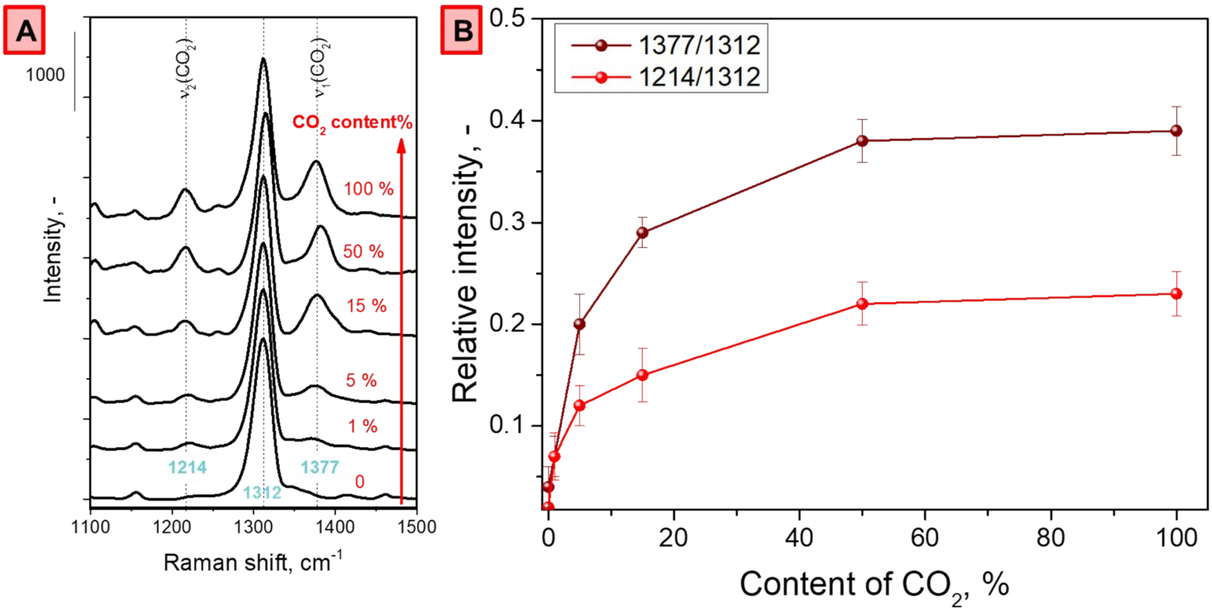

Figure S13 A- SERS spectra of Au-TBD after bubbling with CO_2/N_2 mixtures, B- Dependence of CO_2-related peaks intensity on the CO_2 content.

Schematic representation of experimental set up for atmospheric CO_2 utilisation

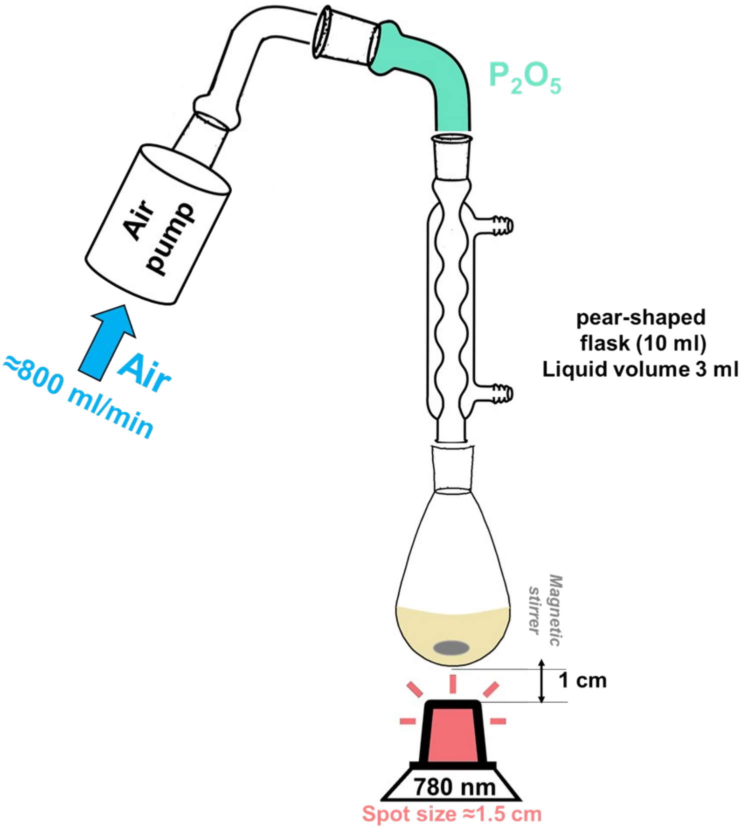

Figure S14 Schematic representation of experimental set up for atmospheric CO_2 utilisation (*entry* 6).

Related discussion

For the plasmon-induced cycloaddition reaction, the 10 ml pear-shaped flask (sodium silicate glass, outer diameter 3 cm, 3.5 cm height, 1mm thick) was filled with the epoxide (3 ml) and Au-TBD (Fig. S13). The LED source (780 nm, 40 mW/cm^2, product number M780LP1, Thorlab) was set up vertically for the distance from LED to the vial to be 1 cm. The spot size of LED was 1.5 cm (emitter size 3 mm) at this distance, and the power "first glass window" was measured to be 40 mW/cm^2 by Integrating Sphere Photodiode Power Sensors (Thorlabs, S142C).

The flask was connected to the reflux condenser to avoid evaporation. The condenser was filled with tube filled with 1.5 g of fresh P_2O_5 (with indicator) to eliminate moisture coming from the air. P_2O_5 filled tube was connected to miniaturized compressor pump (50 l/h, Thomas Oil-less Vacuum Pump), which delivered air instead of pure CO_2. Irradiation and stirring of the reaction mixture were started simultaneously. After 24 hours, the P_2O_5 tube was replaced by freshly filled one. The relative humidity monitoring inside the flask was conducted with humidity equipment with mini probe (UNI-T UT333S, 0.1 RH% resolution, ±2% in 0-100% interval). After 12 hours humidity inside the flask was 0.3 %.

Apparent quantum yield calculation

The apparent quantum yield (**AQY**) was calculated according to the following equation:

$$AQY = \frac{n_{carbonate}}{n_{inced\,photons}} * 100\%, = \frac{41.8 * 10^{-3}}{18.1 * 10^{3}} * 100 = 0.23\ \%,$$

where $n_{carbonate}$ are the moles of formed carbonate and $n_{inced\,photons}$ is the moles of incident photons, at the bottom of flask (at other words – first “reactor” window). The number of incident photons (in moles) was calculated from measured power and averaged photons energy.

References

[S1] Q. W. Song, Z. H. Zhou and L. N. He, *Green Chem.*, 2017, 19, 3707–3728.

[S2] X. Zhang, N. Zhao, W. Wei and Y. Sun, *Catal. Today*, 2006, **115**, 102–106.

[S3] A. Barbarini, R. Maggi, A. Mazzacani, G. Mori, G. Sartori and R. Sartorio, *Tetrahedron Lett.*, 2003, **44**, 2931–2934.

[S4] Z. Z. Yang, Y. N. Zhao, L. N. He, J. Gao and Z. S. Yin, *Green Chem.*, 2012, **14**, 519–527.

[S5] S. Subramanian, J. Oppenheim, D. Kim, T. S. Nguyen, W. M. H. Silo, B. Kim, W. A. Goddard and C. T. Yavuz, *Chem*, 2019, **5**, 3232–3242.

[S6] P. Z. Li, X. J. Wang, J. Liu, J. S. Lim, R. Zou and Y. Zhao, *J. Am. Chem. Soc.*, 2016, **138**, 2142–2145.

[S7] Reid, MT Homer. "Scuff-em: free, open-source boundary-element software."

[S8] Yaws, Carl L. Handbook of Thermal Conductivity, Volume 1: Organic Compounds C1 to C4. Elsevier, 1995.

[S9] www.sigmaaldrich.com/catalog/product/aldrich/241342. (date of access 21.12.2020)

[S10] S. Merabia, S. Shenogin, L. Joly, P. Keblinski and J. L. Barrat, *Proc. Natl. Acad. Sci. U. S. A.*, 2009, **106**, 15113–15118.

[S11] M. T. H. Reid and S. G. Johnson, *IEEE Trans. Antennas Propag.*, 2015, **63**, 3588–3598.

[S12] E. Kazuma and Y. Kim, *Angew. Chemie Int. Ed.*, 2019, **58**, 4800–4808.